

Article

Heat Removal Factor in Flat Plate Solar Collectors: Indoor Test Method

Orlando Montoya-Márquez¹ and José Jassón Flores-Prieto^{2,*}

¹ Facultad de Ingeniería, Universidad Panamericana, Prolongación Calzada Circunvalación Poniente 49, Zapopan 45010, Mexico; ormontoya@up.edu.mx

² Tecnológico Nacional de México—CENIDET. Int. Internado Palmira s/n, Cuernavaca 62490, Mexico

* Correspondence: jasson@cenidet.edu.mx; Tel.: +52-777-362-7770 (ext. 1302); Fax: +52-777-362-7795

Received: 9 August 2018; Accepted: 4 October 2018; Published: 17 October 2018



Abstract: This paper presents a couple of methods to evaluate the heat removal factor F_R of flat plate solar collectors, as well as a parametric study of the F_R against the tilt angle β , and $(T_i - T_a)/G$, and its effects on the a_0 -factor ($F_R \tau \alpha$) and the a_1 -factor ($F_R U_{Lmin}$). The proposed methods were based on indoor flow calorimetry. The first method considers the ratio of the actual useful heat to the maximum useful heat. The second takes into account the slopes of the family of efficiency curves ($F_R U_{Lmin}$) according to ANSI/ASHRAE 93-2010, and the minimum overall heat loss coefficient, U_{Lmin} . In both methods, a feedback temperature control at collector inclinations from horizontal to vertical allows the inlet temperature and the emulating of the solar radiation to be established by electrical heating. The performance of the methods was determined in terms of the uncertainty of the F_R . Method 1 allowed a three-fold improved precision compared to Method 2; however, this implied a more detailed experimental setup. According to the first method, the effects of the tilt angle β , and the $(T_i - T_a)/G$, on the a_0 -factor were considerable, since F_R is directly proportional to the a_0 -factor. The changes in $(T_i - T_a)/G$ caused an average change in F_R of 32%. The F_R shows almost linear behavior for inclinations from horizontal to vertical with a 14.5% change. The effects of β on the a_1 -factor were not considerable, due to the compensation between the increase in F_R and the decrease in U_{Lmin} as β increased.

Keywords: heat removal factor; covered solar collectors; tilt solar collector; inclined solar collector

Highlights

- The effects of tilt angle and $(T_i - T_a)/G$ on the F_R , a_0 -factor and a_1 -factor, were investigated using indoor flow calorimetry.
- The method based on the ratio of the actual useful heat to the maximum useful heat shows considerably improved behavior in terms of uncertainty.
- The F_R shows linear behavior for inclinations from horizontal to vertical with a change of 14.5%.
- The changes in $(T_i - T_a)/G$ caused an average change in F_R of 32%.
- The effect of the variation of the tilt angle and the $(T_i - T_a)/G$ -value on the a_0 -factor is considerable since the F_R is directly proportional to the a_0 -factor.
- The changes in inclination do not considerably affect the a_1 -factor due to the compensation between the increase in F_R and the decrease in U_{Lmin} when β increases.

1. Introduction

In 2014, flat plate collector heating represented 22.4% (83.9 GW_{th}) of the total worldwide solar heating, and this percentage continues to grow [1]. The characterization and simulation have improved

commercialization in many types of process, first for low temperature (<80 °C) and more recently in the medium temperature range (80–250°). The characterization reduces estimating uncertainty and allows better economic scenarios, which are welcome for the solar heating industry.

Flat plate solar collector characterizations are now used to determine the a_0 , a_1 , and the IAM as indicated by [2–6], among other standards and publications. The F_R refers to the thermal effectiveness of solar collectors viewed as heat exchangers, while the a_0 ($F_R \tau \alpha$) is the fraction of the solar radiation GA_a that gains the collector, and the a_1 ($F_R U_{Lmin}$) is the factor of heat losses of the solar collector due to the ambient effect. Most of the solar collector's studies consider the U_{Lmin} as a constant; it is the case in which the efficiency against $(T_i - T_a)/G$ has almost linear behavior. The U_{Lmin} has linear behavior when the efficiency curve is fitted as the second order polynomial approach; however, in this case, the U_{Lmin} is considered a function of $(T_i - T_a)/G$ only. In the same way, the IAM mainly concerns the optical effects of the incidence angle, but does not concern the effect of the confined fluid flow and these optical effects simultaneously, as is the case when U_{Lmin} is considered constant.

The convective flow pattern of the confined fluid between the absorber and the collector glazing is a function of the hot and cold wall temperature changes [7]. In a tilted differentially heated cavity, it has been found that different classes of natural convection flows appear due to changes in tilt angle and the differences in temperature [8–10]. The overall heat transfer coefficient considerably reduces a tall cavity turns from horizontal to vertical [11]. The above-mentioned implies disregarding the fact that the figures of merit F_R , a_0 , and a_1 are a strong function of the U_{Lmin} , which is in turn dependent on the collector inclination due to changes in the difference in outlet–inlet temperature and collector tilt angle. Meanwhile, the influence of collector inclinations mainly takes into account the incidence angle (optical effects: $\tau \alpha$) according to ANSI/ASHRAE 93-2010, 2014 [2]. Awasarmol and Pise [12] studied the natural convection heat transfer from a fin array and angles of inclination. They found a decrease in heat transfer coefficient with the increase in angle of inclination and an optimal angle at 45°. Montoya-Marquez and Flores-Prieto [13] experimentally shows that the changes in collector tilt considerably affects the U_L and the calculations of the efficiency, due to variations in the flow pattern into the air cavity between the absorber plate and glazing.

The F_R is also understood as the ratio of the actual useful heat to the maximum useful heat [4], which is the thermal effectiveness of the solar collector. Thus, one way to show a more detailed picture of the performance or effectiveness of the solar collector, like most heat exchangers, is through the heat removal factor. Currently, the heat removal factor F_R is calculated as the ratio of actual useful energy gains to the useful energy gains, when the whole collector surface is at the fluid inlet temperature. However, this last experimental condition is difficult to achieve because inlet fluid increases its temperature as it flows through the absorber. Additionally, most studies determining F_R have been theoretical, using a combination of thermal parameters, such as the collector fin efficiency factor F' [4]. In addition, the efficiency curve slope at outdoor conditions (a_1 -factor), which is $F_R U_{Lmin}$, can be determined by a standard test [2]. To achieve F_R , the U_{Lmin} must be determined separately.

In line with this, the a_0 -factor and a_1 -factor strongly depend on F_R , but it is usually calculated by a method where U_{Lmin} is considered as a constant or with linear behavior [14–16]. For its part, Malvi et al. [17] reported the performance of a solar flat plate collector for various flow configurations; experiments at indoor conditions were conducted to determine the F_R . The results indicate that, for the same conditions, parallel flow receives a double F_R value compared with the serpentine flow. Experimental methods to evaluate F_R , the a_0 -factor and the a_1 -factor separately, and its uncertainty have an incipient development. On the other hand, the relationships between F_R and β and between F_R and $(T_i - T_a)/G$, which affect the a_0 and a_1 , have become briefly studied, and characterized collectors at a specific latitude have different performance predictions at other latitudes, although these run at the same solar incidence angle. Therefore, the effects of tilt angle β , in a range of $(T_i - T_a)/G$, due to changes in the convective flow patterns, on F_R , which affects the a_0 -factor and a_1 -factor, were experimentally studied by two proposed methods. The tilt collector was studied under inclinations from horizontal to vertical, and a T_i from 60 to 90 °C. The proposed methods were based on indoor

heat flow calorimetry and ANSI/ASHRAE 93-2010 [2]. The indoor condition consideration fixes the solar radiation, ambient temperature, wind velocity, and background radiation, in order to improve the experimental uncertainty.

2. Materials and Method

2.1. Sampling

The study involves the manufacture and instrumentation of the solar collector to work in indoor conditions. The sample is shown in Figure 1; this is a glazing collector with 2.00 m^2 of gross area Aa and an aspect ratio AR of 40. The 10–90% water–glycol is the working fluid, in which heat capacity is considered variable [18]. The absorber is comprised of a couple of header tubes d_1 , and five raised finned tubes d_2 , all of which of copper and joined by tin–lead solder. The absorber solar absorbance α , is 0.94 and the glazing solar transmittance τ is 0.86 [19]. The absorbance and transmittance were obtained by normalizing the measured spectral [20]. A Shimadzu UV-3100 (Shimadzu Corporation, Kyoto, Japan) is used from 300 to 2500 nm, every 2.0 nm with $\pm 0.1\%$ of photometric uncertainty and 1.0% of wavelength uncertainty. Table 1 shows the manufacture characteristics of the sample.



Figure 1. Sample.

Table 1. Manufacture characteristics of the solar collector.

Parameter	Dimension	Units
α	0.94	Dimensionless
τ	0.86	Dimensionless
Aa	1.95×0.95	m
AR	40	Dimensionless
δ	0.003	m
d_1	0.0381	m
d_2	0.0127	m
δa	0.0005	m
W	0.19	m
L_{ins}	0.0254	m

2.2. Experimental Desing

Figure 2 shows that the glazing collector heats up the absorber plate, which in turns heats the working fluid that flows through the raising tubes. At this time, part of the supplied energy $GA\tau\alpha$ heats the working fluid and the rest is transferred to the ambient as heat losses Q_L , which is dependent from the β and $(T_i - T_a)/G$. The incoming heat flux $GA\tau\alpha$ is considered independently of β , and it is the sum of the useful energy $Q_u(\beta, (T_i - T_a)/G)$ plus the heat loss flux $Q_L(\beta, (T_i - T_a)/G)$.

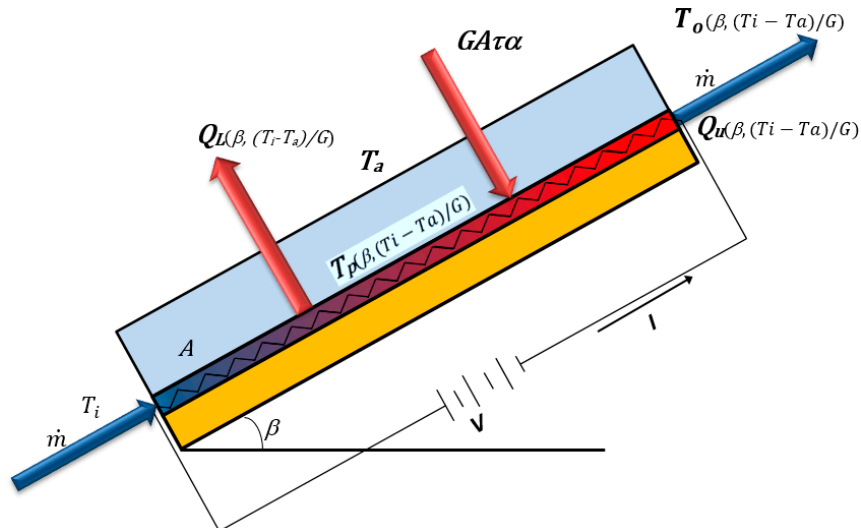


Figure 2. Physical model.

In this study, the incoming heat flux $GA\tau\alpha$ is fixed at a specified value, so the outlet heat is the sum of the actual useful heat $Q_{u,a}(\beta, (T_i - T_a)/G)$, plus the heat loss flux $Q_L(\beta, (T_i - T_a)/G)$. The following considerations are also taken in to account in the experiments: (a) steady state, (b) constant surrounding temperature and emissivity, (c) constant radiative exchange, (d) linear variation of C_p with the temperature, and (e) the mean plate temperature, $T_p(\beta, (T_i - T_a)/G)$, which is considered as the average temperature between outlet and inlet temperature $[T_o(\beta, (T_i - T_a)/G) + T_i]/2$.

The experimental design allows for the determination of the F_R and $F_R U_{L,min}$ as a function of β and $(T_i - T_a)/G$ at indoor conditions by a couple of methods, under inclinations from horizontal to vertical. The a_0 is equal to $F_R \tau \alpha$, and the a_1 is equal to $F_R U_{L,min}$. The indoor condition consideration fixes the solar radiation, ambient temperature, wind velocity, and background radiation, in order to improve the experimental uncertainty. In the first proposed method, the F_R was determined by the ratio of $Q_{u,a}$ to the maximum useful heat $Q_{u,max}$, by indoor flow calorimetry. In the second proposed method, the $F_R U_{L,min}$ was determined according to ANSI/ASHRAE 93-2010 [2] by achieving the slopes of the families of the efficiency curves, and the $U_{L,min}$ by flow calorimetry at indoor conditions too. The indoor condition is the main difference of the second method with the standard technique to obtain the factor $F_R U_{L,min}$. In both proposed methods, a feedback temperature control works at a set of collector inclinations from horizontal to vertical. At indoor conditions, the solar heating was emulated by the Joule effect and the PID control, using an electrical heater, making it possible to replace $(T_i - T_a)/G$ by $(T_i - T_a)/(VI/A\tau\alpha)$, to achieve better experimental uncertainty. Thus, the solar heating is given by Equation (1):

$$GA = \frac{VI}{\tau\alpha} \quad (1)$$

where τ and α are the glazing solar transmittance and the solar absorbance of the absorber respectively, and V and I are the electrical voltage and current, respectively. The performance of both methods was evaluated in terms of uncertainty, which was determined by the propagation error method and by the RMSE and R_2 , respectively.

Method 1: F_R as a Function of the Ratio $Q_{u,a}/Q_{u,max}$

Equation (2) shows that the F_R is the ratio of the actual useful heat to the maximum useful heat, according to Duffie and Beckman [4]. The $Q_{u,max}$ occurs when T_p is equal to T_i , or T_o is equal to T_i , because Q_L tends to be minimal. In the case, that T_p or T_o is greater than T_i , the Q_L is greater than zero, and the $Q_{u,a}$ is then greater than zero too.

$$F_R = \frac{Q_{u,a}(\beta, (T_i - T_a)/G)}{Q_{u,max}(\beta, (T_i - T_a)/G)} \tag{2}$$

The $Q_{u,a}(\beta, (T_i - T_a)/G)$ can be correlated by the change in enthalpy of the working fluid between outlet and inlet, at constant pressure. The $Q_{u,max}$ occurs when the whole collector is at the inlet fluid temperature, minimizing heat losses, $Q_{L,min}$. For this, $T_p = T_i$, or $T_o = T_i$, as is shown in Equation (3).

$$F_R = \frac{Q_{u,a}(\beta, (T_i - T_a)/G)}{A[G\tau\alpha - U_{L,min}(T_i - T_a)]} \tag{3}$$

The F_R value is determined by two parallel tests. The first determines the $Q_{u,a}$ at a fixed value of $GA\tau\alpha$. In the second, the $Q_{L,min}$, and the $Q_{u,max}$, are determined considering $T_p = T_i$ and adjusting the $GA\tau\alpha$. In this case, the F_R is a function of β and $(T_i - T_a)/G$, as well as $Q_{u,a}$, $Q_{L,min}$ or $(VI)_2$, $Q_{u,max}$, and T_p , as is shown in Figure 3.

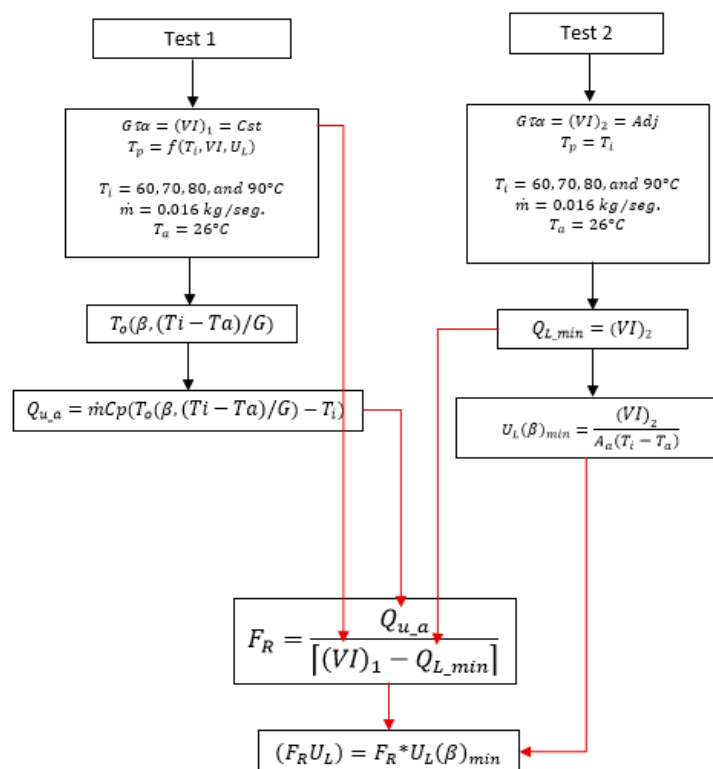


Figure 3. Mathematical model.

Method 2: $F_R U_{L,min}$ According to ANSI/ASHRAE 93-2010

The $F_R U_{L,min}$ was determined based on ANSI/ASHRAE 93-2010 [2], the $U_{L,min}$ factor was obtained separately, using heat flow calorimetry as per Beikircher et al. [3] and Montoya-Marquez and Flores-Prieto [13]. A set of tests is used to determine the family of efficiency curves against $(T_i - T_a)/G$, at inclinations from horizontal to vertical, which in turn allows for a set of $F_R U_{L,min}$, each of which represents the slope of linear regression of each efficiency curve. The $U_{L,min}$ is determined to achieve the

value of the F_R once the $F_R U_{L_{min}}$ is achieved by Method 1 (Test 2), setting the $GA\tau\alpha$ as the compensation heat flux $(VI)_2$ and setting the difference in temperature $(T_i - T_a)$ according to Equation (4):

$$U_{L_{min}} = \frac{(VI)_2}{A_a(T_i - T_a)}. \quad (4)$$

Equation (5) gives the collector efficiency (ANSI/ASHRAE 93-2010, 2014) [2]:

$$\eta\left(\beta, \frac{T_i - T_a}{G}\right) = \frac{Q_u\left(\beta, \frac{T_i - T_a}{G}\right)}{\left(\frac{VI}{A\tau\alpha}\right)}. \quad (5)$$

2.3. Experimental Setup

The experimental setup entails that the sample is mounted with a variable angle β at 0–90°, with an uncertainty of $\pm 0.1^\circ$. The absorber heating (VI) is homogeneously distributed by means of the electrical heater and remains almost constant over each test. The electrical heater is supplied with a maximum of 2000 W, with an uncertainty of ± 5 W. The temperature differences $(T_o - T_i)$ and $(T_i - T_a)$ were measured using a thermopile type T thermocouple and 32 gauge wires, with an uncertainty of $\pm 0.1^\circ\text{C}$. A thermal bath supplied with a 10–90% water–glycol mixture was used as working fluid, with an uncertainty of $\pm 0.01^\circ\text{C}$. The mass flow rate was 0.016 kg/s [21,22]; it was monitored with a turbine flowmeter, with an uncertainty of 3%. It was also verified by weighing the water–glycol mixture, at specified time steps during the experiments. The experimental setup is shown in Figure 4.

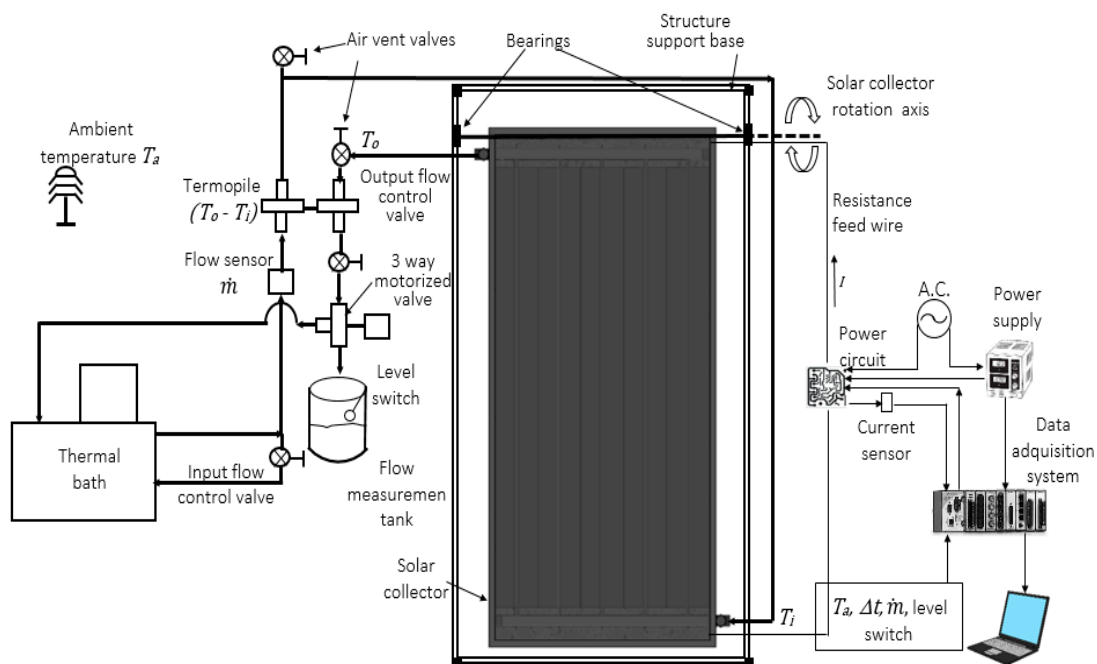


Figure 4. Experimental setup.

The experimental indoor conditions allow uniform surrounding temperature and surrounding emissivity, and the experiments can be run with non-considerable changes in solar heating, ambient temperature, and wind velocity. The working fluid was a 10–90% water–glycol mixture to minimize adverse boiling effects. A programmable FPGA (NI-cRIO9022, 32 bit data acquisition, Lab-VIEW software) (National Instruments, Austin, TX, USA) was used to monitor, record, and calculate the experimental variables at time steps of 1 s. The steady state was verified by monitoring experimental data without considerable changes in the experimental variables over 30 min. Each reported data point corresponds to an average of over 1800 measurements, taken over a 30 min period. The tests

were run at a specified range and steps of the tilt angle, and the remaining variables involved in the experiment were considered without significant variations. Each test was carried out by in triplicate for comparison.

The experimental conditions $T_p = T_i$ and $T_p = f(T_i, VI, U_L)$ was verified by infrared imaging on the absorber plate. As seen in Figure 5, the field temperature of the absorber plate was as expected, thanks to the PID control losses compensation. Figure 5a shows the $T_p = T_i$ condition, where the standard deviation was only 0.14 °C. Figure 5b shows the case in which $T_p = f(T_i, VI, U_L)$, where we can find a conventional temperature profile of the solar collector absorber.

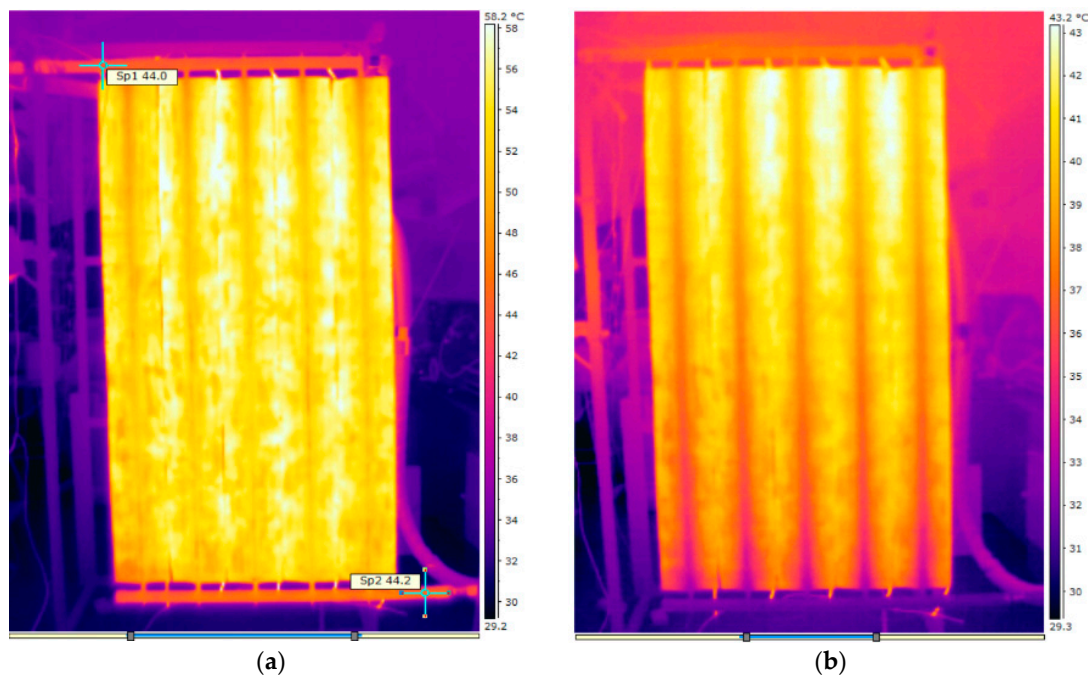


Figure 5. Infrared imaging testing of the absorber plate at the (a) $T_p = T_i$ and (b) $T_p = f(T_i, VI, U_L)$.

3. Results

The experiments were conducted highlighting the behavior of the F_R and $F_R U_{Lmin}$ as a function of the β and $(T_i - T_a)/G$. As noted above, the a_0 -factor is direct proportional to F_R and the a_1 -factor is equal to $F_R U_{Lmin}$. The experimental campaign comprises five sets of four experiments, each one performed in triplicate. The parametric study was conducted for β as follows: 0°, 30°, 45°, 60°, and 90°. The $(T_i - T_a)/G$ was 0.044, 0.056, 0.069, and 0.083.

3.1. Comparative Performance of both Methods

The uncertainty, in terms of $RMSE$ and R_2 , of each method disclose its performance. Figure 6 shows a similar shape of F_R against β for both methods. The F_R grew were 0.14 and 0.27 for Methods 1 and 2, respectively. The experimental uncertainties of Methods 2 and 1 were ± 0.049 and ± 0.016 respectively; this is 306% times greater with Method 2 compared with Method 1. As seen in Figure 6, both shadow gaps of the experimental uncertainty are cross practical. The linearity values are (0.053, 0.9630) and (0.104, 0.9708) for Methods 1 and 2, respectively. The $RMSE$ was considerably higher in Method 2. Method 1 allows for achieving an F_R value for every studied value of $(T_i - T_a)/G$, unlike Method 2, where the F_R is just an average value determined from the slope of each efficiency curve. Therefore, the remainder of this paper focuses on Method 1.

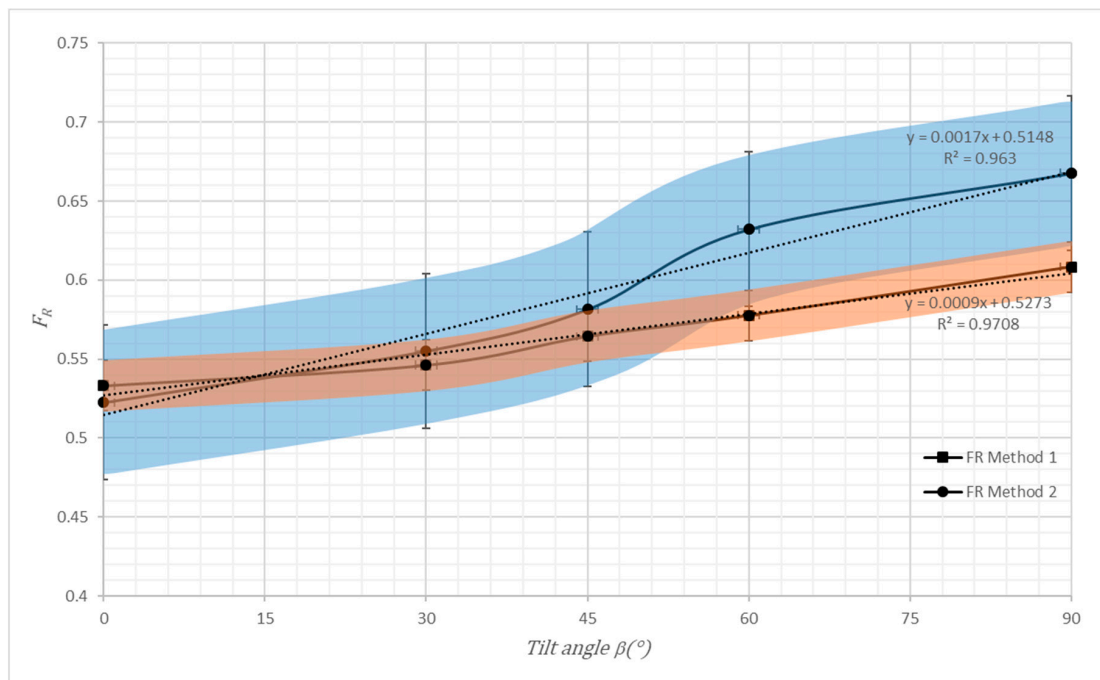


Figure 6. The F_R against β by Methods 1 and 2.

3.2. Method 1: F_R , $a_1:F_R U_{Lmin}$ and U_{Lmin} against β

Figure 7 shows the F_R , U_{Lmin} and $(F_R U_{Lmin})$ against β based on Method 1, taking the average values over the set of $(T_i - T_a)/G$. The F_R increases from 0.34 to 0.61 (14.5%) as the angle of inclination increases from 0 to 90°. The F_R increases as it goes from horizontal to vertical; this is because U_{Lmin} decreases its value at the same time, from 5.9 to 5.4 $W/m^2 \cdot K$. The increase in F_R and the decline of U_{Lmin} cause $F_R U_{Lmin}$ to remain almost constant along the inclination set of tests, changing only 0.1 $W/m^2 \cdot K$ (3.0%). Thus, the coefficient a_1 , of the solar collector efficiency curve, does not change considerably with the inclination angle. In addition, the coefficient a_0 can change considerably if the $\tau\alpha$ remains almost constant.

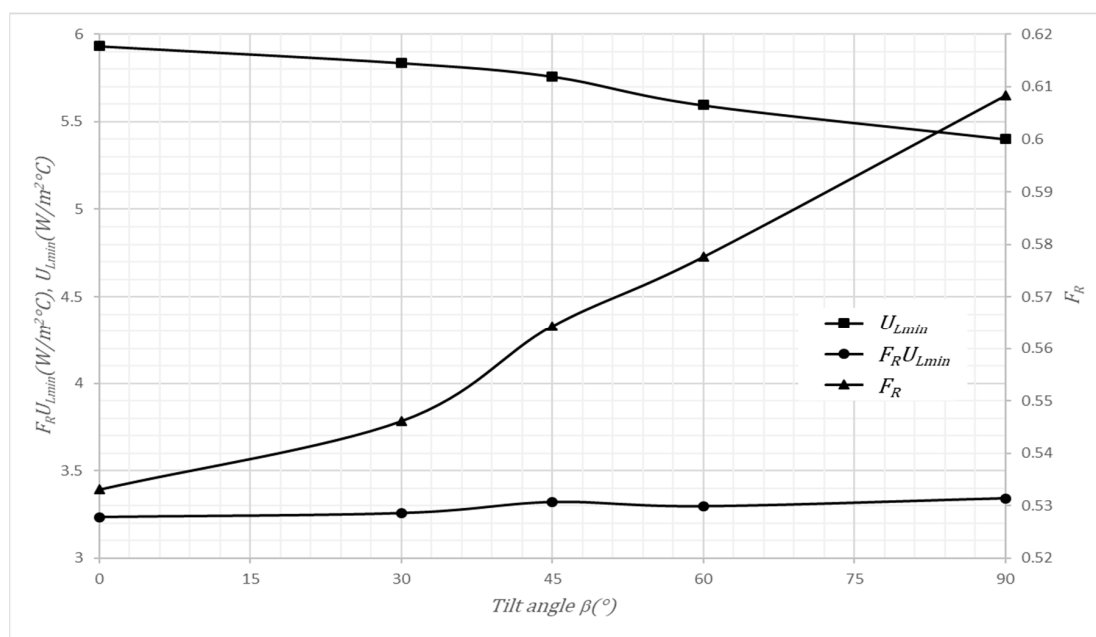


Figure 7. F_R , $a_1:F_R U_{Lmin}$ and U_{Lmin} against β by Method 1.

3.3. Method 1: $F_R, a_1:F_R U_{Lmin}$ against β and $(T_i - T_a)/G$

Figure 8 shows F_R against β for the studied range of $(T_i - T_a)/G$. The change in F_R was 14.5% on average over the set of β , as mentioned above. On the other hand, the variation of $(T_i - T_a)/G$ means average changes in F_R of 32% over the set of $(T_i - T_a)/G$, and the a_0 is affected considerably due to changes in $(T_i - T_a)/G$, only if $\tau\alpha$ remains almost constant, because the flow pattern between the absorber plate and glassing cover is modified considerably. The latter is in the same line of the experimental work of Montoya-Marquez and Flores-Prieto [13].

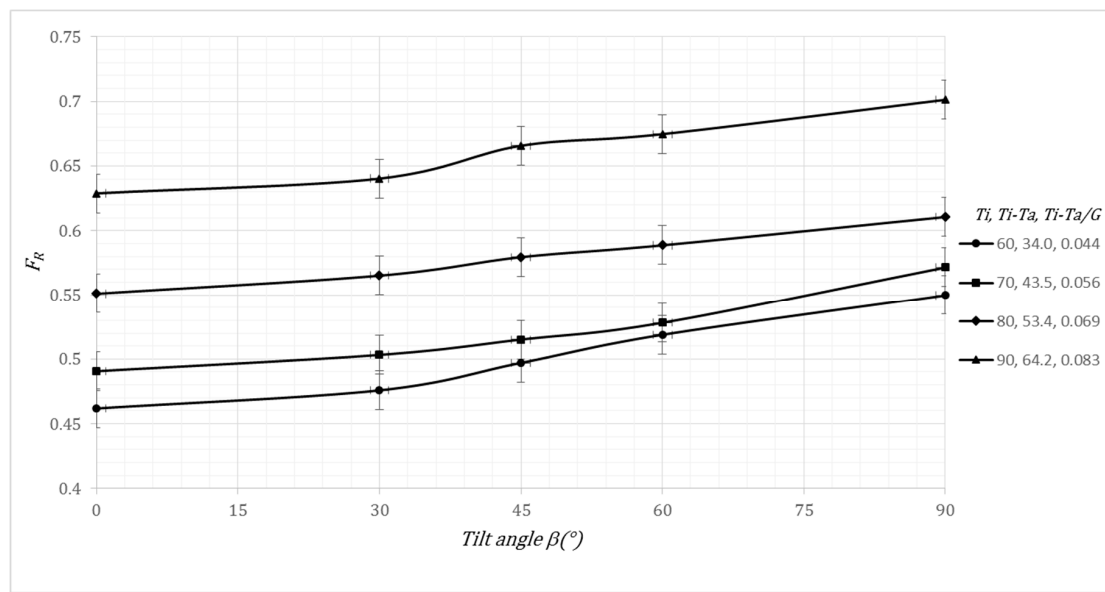


Figure 8. F_R vs. β and $(T_i - T_a)/G$ by Method 1.

Figure 9 shows $a_1:F_R U_{Lmin}$ as a function of β and $(T_i - T_a)/G$ for Method 1. The a_1 -factor shows variations over the set of β that are not considerable. However, the a_1 -factor can change by 2.3% over the studied range of $(T_i - T_a)/G$. Over the range of $(T_i - T_a)/G$, the changes in a_1 -factor as a function of β is not considerable due to the compensation between the increase in F_R and the decrease in U_{Lmin} when β increases.

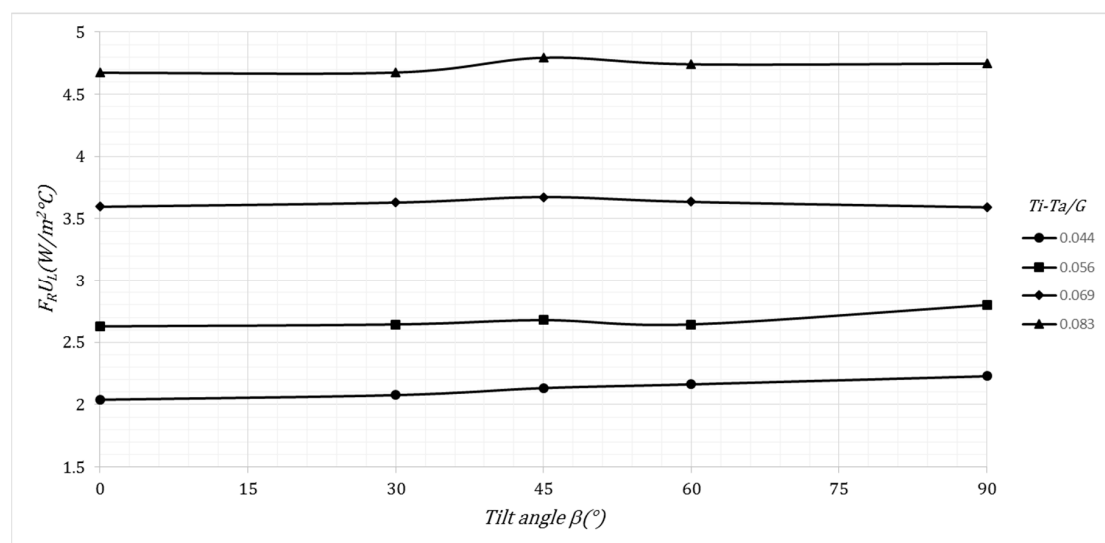


Figure 9. The $a_1:F_R U_{Lmin}$ as a function of β and $(T_i - T_a)/G$ by Method 1.

4. Conclusions

A couple of experimental indoor test methods for determining F_R and $F_R U_{Lmin}$ (a_1 -factor) were conducted. Method 1 determined the ratio of $Q_{u,a}$ to $Q_{u,max}$; Method 2, by achieving the slopes, determined the $F_R U_{Lmin}$ of the family of the efficiency curves, (ANSI/ASHRAE 93-2010, 2014) [2] and the U_{Lmin} by indoor flow calorimetry. The effects of tilt angle and $(T_i - T_a)/G$ on the F_R and $F_R U_{Lmin}$ factors were investigated, considering that the a_0 is directly proportional to F_R and a_1 is equal to $F_R U_{Lmin}$. Both methods determine the behavior of F_R against tilt angle and $(T_i - T_a)/G$. However, Method 1 shows considerably improved behavior in terms of uncertainty of F_R —a three-fold lower uncertainty. Thus, a method was conducted to obtain the F_R with the use of a PID temperature control at fixed indoors conditions, with which it is possible to obtain the F_R with lower uncertainty. In addition, Method 1 shows some advantages over Method 2—more data points, less uncertainty, and a complete view of the collector's efficiency—but a more detailed experimental setup is needed.

The changes in inclination from horizontal to vertical caused an almost linear increase in F_R , (14.5%), which represents a change of 45% due to $(T_i - T_a)/G$, which caused an average change in F_R of 32%. Thus, the effects of changes in tilt angle and $(T_i - T_a)/G$ -value on the a_0 -factor is considerable, since a_0 is directly proportional to F_R . The inclination changes do not considerably affect the a_1 -factor due to the compensation between the increase in F_R and the decrease in U_{Lmin} when β increases.

Author Contributions: O.M.-M. and J.J.F.-P. contributed to the design and implementation of the research, to the analysis of the results and to the writing of the manuscript.

Funding: This research was funded by Consejo Nacional de Ciencia y Tecnología México, CONACyT and the Tecnológico Nacional de México (Project. 5685.16), and the APC was funded by the Tecnológico Nacional de México.

Acknowledgments: The authors are grateful to Consejo Nacional de Ciencia y Tecnología, CONACyT and Tecnológico Nacional de México, TecNM, whose financial support made this work possible.

Conflicts of Interest: The authors declare that they have no conflict of interest.

Nomenclature

Variables	Description	Units
A_a	Collector area	m^2
AR	Aspect ratio	-
C_p	Specific heat	$kJ/kg \cdot K$
d_1	Diameter of heaters	m
d_2	Diameter of raising tubes	m
F_R	Heat removal factor	Adimensional
G	Solar radiation	W/m^2
IAM	Incidence angle modifier	-
L_{ins}	Insulation width	m
\dot{m}	Mass flow	kg/s
Q_i	Input heat	W
Q_l	Loss heat	W
Q_u	Useful heat	W
$Q_{u,a}$	Actual useful heat	W
$RMSE$	Root mean square error	-
R_2	Coefficient of determination	Adimensional
T_a	Ambient Temperature	$^\circ C$
T_i	Input temperature	$^\circ C$
T_o	Output temperature	$^\circ C$
T_p	Mean absorber plate temperature	$^\circ C$
U_L	Overall heat transfer coefficient	$W/m^2 \cdot ^\circ C$
VI	Electric power	W
W	fin width	m

Symbols

α	Absorbance	Adimensional
β	Tilt angle	°
δ	Glass cover thickness	m
δ_a	Fin thickness	m
τ	Transmittance	Adimensional
η	Efficiency	Adimensional

References

- Mauthner, F.; Weiss, W.; Spörk-Dür, M. *Solar Heat Worldwide*; IEA Solar Heating & Cooling Programme: Gleisdorf, Austria, 2016.
- American Society of Heating, Refrigerating, and Air-Conditioning Engineers, Inc. *Methods of Testing to Determine the Thermal Performance of Solar Collectors*; ANSI/ASHRAE 93-2010 (RA 2014); ASHRAE: Atlanta, GA, USA, 2014.
- Beikircher, T.; Osgyan, P.; Fischer, S.; Drück, H. Short-term efficiency test procedure for solar thermal collectors based on heat loss measurements without insolation and a novel conversion towards daytime conditions. *Sol. Energy* **2014**, *107*, 653–659. [[CrossRef](#)]
- Duffie, J.; Beckman, W. *Solar Engineering of Thermal Processes*, 4th ed.; John Wiley & Sons, Inc.: Hoboken, NJ, USA, 2013.
- International Standard, Test Methods for Solar Collectors—Part 1: Thermal Performance of Glazed Liquid Heating Collectors Including Pressure Drop*; ISO 9806-1; ISO: Vernier, Switzerland, 1994.
- Sabatelli, V.; Marano, D.; Braccio, G.; Sharma, V.K. Efficiency test of solar collectors: Uncertainty in the estimation of regression parameters and sensitivity analysis. *Energy Convers. Manag.* **2002**, *43*, 2287–2295. [[CrossRef](#)]
- Saury, D.; Benkhelifa, A.; Penot, F. Experimental determination of first bifurcations to unsteady natural convection in a differentially-heated cavity tilted from 0° to 180°. *Exp. Therm. Fluid Sci.* **2012**, *38*, 74–84. [[CrossRef](#)]
- Alvarado, R.; Xamán, J.; Hinojosa, J.; Álvarez, G. Interaction between natural convection and surface thermal radiation in tilted slender cavities. *Int. J. Therm. Sci.* **2008**, *47*, 355–368. [[CrossRef](#)]
- Ozoe, H.; Sayama, H.; Churchill, S.W. Natural convection in an inclined rectangular channel at various aspect ratios and angles—Experimental measurements. *Int. J. Heat Mass Transf.* **1975**, *18*, 1425–1431. [[CrossRef](#)]
- Ozoe, H.; Yamamoto, K.; Sayama, H.; Churchill, S.W. Natural convection in an inclined rectangular channel heated on one side and cooled on the opposing side. *Int. J. Heat Mass Transf.* **1974**, *17*, 1209–1217.
- Cooper, P.I. The effect of inclination on the heat loss from flat-plate solar collectors. *Sol. Energy* **1981**, *27*, 413–420. [[CrossRef](#)]
- Awasarmol, U.V.; Pise, A.T. An experimental investigation of natural convection heat transfer enhancement from perforated rectangular fins array at different inclinations. *Exp. Therm. Fluid Sci.* **2015**, *68*, 145–154. [[CrossRef](#)]
- Montoya-Marquez, O.; Flores-Prieto, J.J. The effect of the angle of inclination on the efficiency in a medium-temperature flat plate solar collector. *Energies* **2017**, *10*, 71. [[CrossRef](#)]
- Kumar, P.; Roy, S.C.; Paswan, M.K. Experimental study of Collector heat removal factor and Collector efficiency factor of flat-plate solar Air Heater having roughened (Rhombus shape) absorber plate. *Int. J. Tech. Res. Appl.* **2016**, *4*, 170–174.
- Rosli, M.A.M.; Misha, S.; Sopian, K.; Mat, S.; Sulaiman, M.Y.; Salleh, E. Parametric analysis on heat removal factor for a flat plate solar collector of serpentine tube. *World Appl. Sci. J.* **2014**, *29*, 184–187.
- Xie, W.T.; Dai, Y.J.; Wang, R.Z. Theoretical and experimental analysis on efficiency factors and heat removal factors of Fresnel lens solar collector using different cavity receivers. *Sol. Energy* **2012**, *86*, 2458–2471. [[CrossRef](#)]
- Malvi, C.S.; Gupta, A.; Gaur, M.K.; Crook, R.; Dixon-Hardy, D.W. Experimental investigation of heat removal factor in solar flat plate collector for various flow configurations. *Int. J. Green Energy* **2017**, *14*, 442–448. [[CrossRef](#)]

18. Lyondell Chemical Company. Technical Data Propylene Glycol Boiling Point of Aqueous Propylene Glycol Solutions 2006. Available online: <http://www.lyondellbasell.com/techlit/techlit/2519.pdf> (accessed on 4 April 2013).
19. CIE 130-1998, *Practical Methods for the Measurement of Reflectance and Transmittance*; Technical Report No. 130; Commission Internationale de L'Eclairage: Vienna, Austria, 1998.
20. *Glass in Building—Determination of Light Transmittance, Solar Direct Transmittance, Total Solar Energy Transmittance, Ultraviolet Transmittance and Related Glazing Factors*; ISO9050-2003; ISO: Vernier, Switzerland, 2003.
21. Bava, F.; Furbo, S. *Correction of Collector Efficiency Depending on Variations of Collector Type, Solar Collector Fluid, Volume Flow Rate and Collector Tilt*. IEA-SHC Info Sheet 45.A.1. 22 December 2014. Available online: <http://task45.iea-shc.org/data/sites/1/publications/IEA-SHC-T45.A.1-INFO-Correctionofcollector-efficiency.pdf> (accessed on 21 December 2016).
22. Zauner, C.; Hengstberger, F.; Hohenauer, W.; Reichl, C.; Simetzberger, A.; Gleiss, G. Methods for medium temperature collector development applied to a CPC collector. *Energy Procedia* **2012**, *30*, 187–197. [CrossRef]



© 2018 by the authors. Licensee MDPI, Basel, Switzerland. This article is an open access article distributed under the terms and conditions of the Creative Commons Attribution (CC BY) license (<http://creativecommons.org/licenses/by/4.0/>).